Upcycling atmospheric CO_2 to polyhydroxyalkanoates via sequential chemo-biocatalytic processes

Manuel Bruch[1,2†], Julian E. Sanchez-Velandia[3†], Jhonatan Rodríguez-Pereira[4,5], Michelle Rich[6], Nicole Pearcy[6], Tanja Narančić[1,2], Eduardo Garcia-Verdugo[3], Victor Sans[7], Kevin O'Connor[1,2*], Marcileia Zanatta[7,8*]

1. School of Biomolecular and Biomedical Sciences, University College Dublin, Dublin, Ireland
2. BiOrbic, Bioeconomy SFI Research Centre, Dublin, Ireland
3. Departamento de Quimica Inorganica y Organica, Avda Sos Baynat, s/n, 12071 Castelló de la Plana, Spain
4. Center of Materials and Nanotechnologies, Faculty of Chemical Technology, University of Pardubice, Nam. Cs. Legii 565, 53002 Pardubice, Czech Republic
5. Central European Institute of Technology, Brno University of Technology, Purkynova 123, 61200 Brno, Czech Republic
6. BBSRC/EPSRC Synthetic Biology Research Centre (SBRC), University of Nottingham, University Park, Nottingham, NG7 2RD, United Kingdom
7. Institute of Advanced Materials (INAM), Universitat Jaume I (UJI), Avda Sos Baynat, s/n, 12071 Castelló de la Plana, Spain
8. Departament de Química Física i Analítica, Universitat Jaume I, Avda Sos Baynat s/n, 12071 Castelló de la Plana, Spain

† These authors contributed equally to the work.

* zanatta@uji.es, kevin.oconnor@ucd.ie

Abstract

The reduction of greenhouse gas emissions and the shift away from petrochemical-derived materials are critical goals in modern industrial development and societal progress. Addressing these intertwined challenges demands innovative and sustainable solutions. Here, we present the first example of synthesizing poly[*R*-(–)-3-hydroxybutyrate] (PHB) from atmospheric CO_2, utilizing a streamlined and integrated process that combine both chemo- and biocatalytic conditions. Central to our approach is the development of an immobilized catalytic system that efficiently converts atmospheric CO_2 into sodium formate, establishing a sustainable carbon source for formatotrophic organisms. Through Adaptive Laboratory Evolution (ALE), we enhanced the growth rate of the bacterium *Cupriavidus necator* H16, enabling it to utilize formic acid and formate as the sole carbon and energy sources. The evolved strain, *C. necator* ALE26, achieved a 1.8-fold increase in maximum growth rate ($\mu max = 0.25 \pm 0.02\ h^{-1}$), attributed to the loss of the megaplasmid pHG1. Employing the adapted

strain, we report the highest PHB production rate in continuous fermentation using *C. necator* for growth on formate. The development of the different stages (sorption, chemo- and biotransformation) under compatible conditions that minimize the number of work-up stages demonstrates a major advancement in converting atmospheric CO_2 into valuable biopolymers, thus simultaneously contributing to the reduction of greenhouse gases in the atmosphere and to a circular economy of biobased polymers that diminish fossil fuel dependence.

Table of content

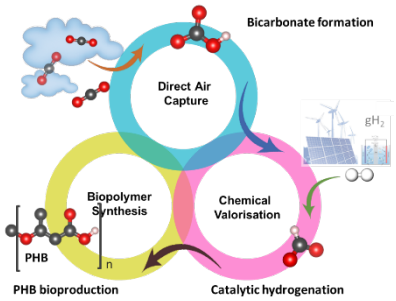

From atmospheric CO_2 to green plastics, a sustainable journey.

Highlights

- First example of the synthesis of PHB from atmospherically captured CO_2.
- Streamlined process with compatible conditions for the sorption, chemo- and biocatalytic transformations.
- Development of a novel immobilised catalytic system to transform atmospheric CO_2 to formate.
- Highest PHB production rate in a continuous fermentation from formate via adaptive laboratory evolution strategies.
- Continuous-flow biocatalytic PHB generation employing chemo-catalytically generated formate.

Introduction

Climate change is one of the major global challenges of the 21st century.[1-4] The increasing concentration of carbon dioxide (CO_2) in the atmosphere is a major driver of climate change, necessitating innovative solutions for its capture and reuse.[5] Currently only 1.3 % of the total annual CO_2 emission are captured.[1, 2] For post-combustion carbon capture, two strategies are

highlighted in carbon capture, utilisation and storage (CCUS) and direct air capture (DAC). The former aims to strip carbon from flue gas from industrial processes and is generally more energy efficient due to the higher carbon concentrations in these gas streams compared to ambient air. However, it has long been argued that to truly achieve a carbon negative economy, historically emitted carbon needs to be recaptured from the atmosphere, leading to a growing interest in DAC technologies.[6, 7] Efficient direct air capture and integrated conversion (DACC) processes offer a promising opportunity to address these challenges by removing CO_2 directly from the atmosphere and converting it into added-value products.[8]

Current state-of-the-art chemical DACC technologies for CO_2 hydrogenation reaction primarily focus on production of C_1 compounds such as methanol, methane or formate salts.[9-19] In this process, the DAC step is typically performed using amines or hydroxides, which generate carbamate or carbonates species that are subsequently hydrogenated to the desired product.[8] In the conversion step, the hydrogenation to formate is particularly interesting due to its potential for further upgrading to higher added-value CO_2-derived synthetic products.[20] Among the notable catalytic systems for the hydrogenation of carbonate/carbamates to formate, the most employed are iridium (Ir) and ruthenium (Ru)-based complexes.[21-23] Despite significant advances in DACC technology, several critical challenges remain. One of the primary issues is the difficulty in recycling catalysts and, more significantly, the adsorbents, which are predominantly used in the homogeneous phase. This usage complicates their recovery and reuse, thereby reducing the overall efficiency and sustainability of the process. Additionally, the limited usability of the final products further restricts the practical applications of DAC.[8] Thus, it is crucial to design efficient reaction and product separation processes, as well as systems for the recovery and reuse of all reaction elements, including catalysts and adsorbents. Additionally, to maximize their impact and to reduce the fossil fuel dependence, it is essential to enhance the added value of the products generated from captured CO_2, moving beyond simple C_1-C_2 products to more complex and valuable chemicals.

In this context, biology emerges as a promising avenue for transitioning from C_1 to C_n products derived from CO_2. Many organisms including plants and a plethora of bacteria can utilise CO_2 and/or other C_1-gases as carbon sources to produce complex molecules, such as sugars, alcohols, lipids, pharmaceutically active ingredients and polymers.[24-26] Energy is either derived from light (photosynthesis) or inorganic molecules like molecular hydrogen (H_2). Photosynthetic solutions become difficult at large scales when even lighting needs to be provided for efficient production processes. Working with CO_2 and H_2 directly in microbial fermentations requires elaborate set-ups to avoid the risk of explosions, especially if the organism used is grown aerobically. Furthermore, both CO_2 and H_2 suffer from low water solubility although much research has been dedicated to tackling this challenge through

process engineering.[27, 28] Thus, alternative strategies for providing carbon and hydrogen to the biological catalyst can improve these processes. Chemical CO_2 fixation therefore can be a key step in providing easily accessible carbon sources for microbial fermentations.

For decades, the Gram-negative bacterium *Cupriavidus necator (C. necator)* H16 has been investigated for its capabilities of growing on CO_2 as its sole carbon source and as a model organism to produce the biodegradable polyester poly[*R*-(–)-3-hydroxybutyrate] (PHB), with properties similar to polypropylene.[29-34] It naturally uses H_2 as its energy source in autotrophic growth. Recently, studies in simple batch set-ups have investigated *C. necator*'s PHB production capabilities in true autotrophy on gaseous feedstocks,[35, 36] focussing on different factors in cell growth and PHB accumulation.[37] Alternatively, in a CCUS context, CO_2 from flue gas has been used together with *in situ* electrochemical hydrogen generation to accumulate PHB in the bacterium.[38] The same group has developed a two-stage process in which compressed CO_2 is first electrochemically reduced to formate which in turn is fed to resting *C. necator* cells for PHB accumulation.[39]

In recent years, the use of formic acid and formate salts as an alternative carbon source for a group of bacteria coined "formatotrophs" has been popularised.[37, 40] However, to date, the integration of DAC technologies and biotechnological product formation however, remains unexplored. Chemical synthesis of formic acid or formate salts can provide a readily available, water-soluble alternative C_1 carbon source for *C. necator*. Here we introduce an innovative synthetic route to produce PHB that integrates three key processes: DAC of CO_2, chemo-catalytic hydrogenation, and biocatalytic transformation (**Figure 1).** To the best of the authors' knowledge, this is the first example of production of the commercially viable product PHB from captured atmospheric air and also fist example of continuous fermentation for accumulation of PHB from formate. Our primary objective was two-fold: i) to showcase the conversion of atmospheric CO_2 into formate salts under conditions compatible with further bioprocessing steps and ii) to optimize the growth and polyhydroxybutyrate (PHB) accumulation of *C. necator* on formic acid/formate in a continuous bioprocess via Adaptive Laboratory Evolution (ALE) and process optimisation. This integrated approach not only demonstrates the feasibility of converting CO_2 into useful products but also highlights the potential for sustainable and economically viable processes that can help reduce fossil fuel dependence and mitigate climate change.

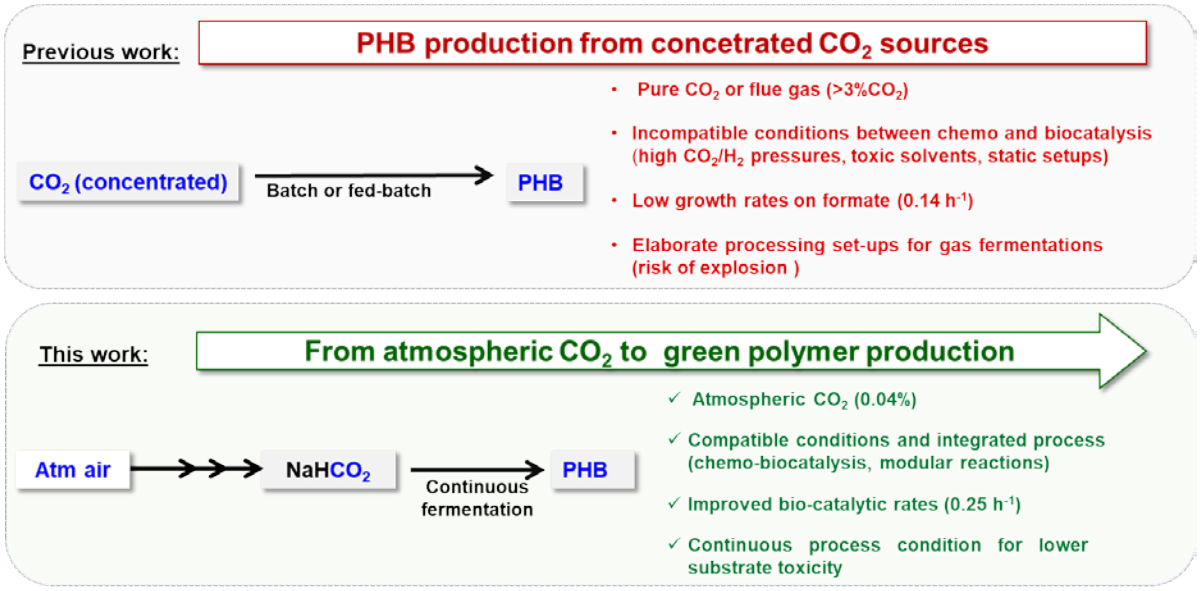

Figure 1. State of the art and our approach.

Results and discussion

Hydrogenation of atmospheric CO_2 to formate

The CO_2 molecule, in its gaseous form, exhibits sp hybridisation, resulting in a strong overlap of bonding orbitals that inherently limits its reactivity. However, when subjected to chemical capture processes, CO_2 adopts a more reactive configuration, specifically a trigonal planar sp^2 hybridisation, as seen in bicarbonate (HCO_3^-) and carbamates. When formed from CO_2, bicarbonate has a reaction enthalpy of -45 kJ/mol, compared to carbamate (-80 kJ/mol).[41] Thus, bicarbonate is a more accessible and reactive intermediate and to be further transformed into added value products. Therefore, our previous research demonstrated the feasibility of DAC coupled with sequential cyclic carbonates.[42] In this study, we chose to utilize water for DAC, rather than organic solvents, due to its environmentally friendly properties and compatibility with subsequent biological processes (**Figure 2A**). Tetrabutylammonium hydroxide (TBA.OH) and sodium hydroxide (NaOH) were tested as capture agents for atmospheric CO_2 (**Figure 2B**). The choice of TBA (tetrabutylammonium) as the preferred cation for CO_2 capture is based on our previous work, where it demonstrated superior efficiency compared to other organic salts, such as cholinium, phosphonium, and imidazolium.[42] TBA has shown the ability to capture CO_2 and convert it into $TBAHCO_3$, which can then be used in the synthesis of industrial chemicals like PHB. Analysis depicted in **Figure 2C** revealed that TBA.OH yielded $TBA.HCO_3$, as evidenced by a signal at 161 ppm in the ^{13}C NMR spectrum, whereas sodium hydroxide yielded carbonate (Na_2CO_3) species, indicated by a signal at 168 ppm in the ^{13}C NMR spectrum. Furthermore, under these conditions, the TBA.OH exhibited an optimal sorption capacity, by fully transforming into $TBA.HCO_3$. Moreover, our findings indicate the scalability of the process to 100 mL scale.

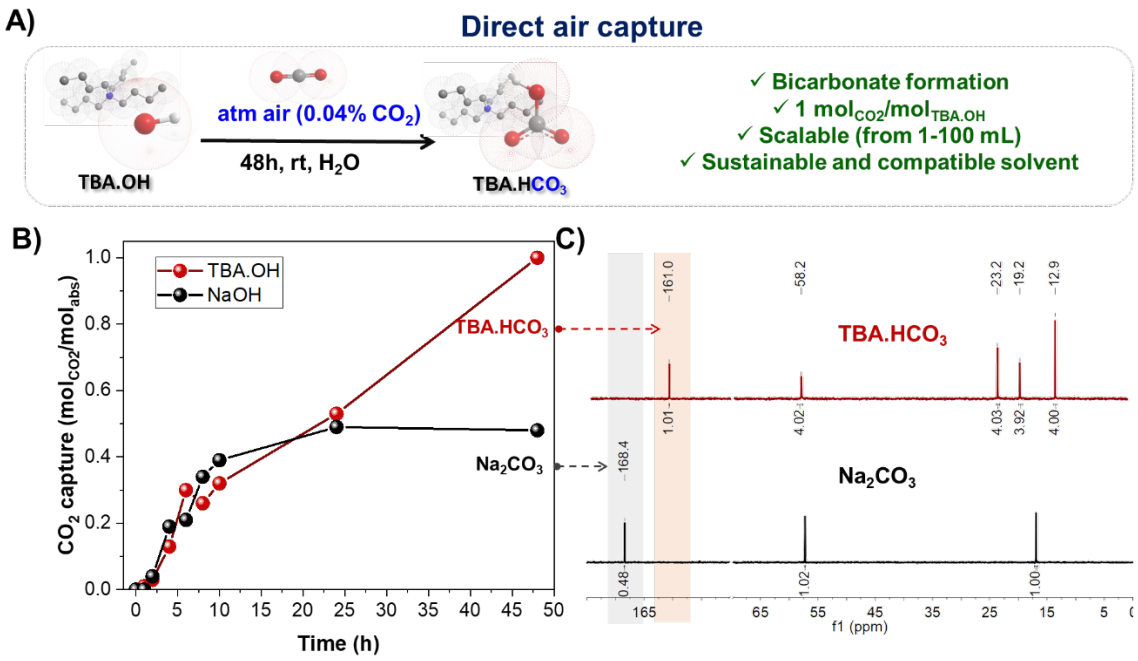

Figure 2. DAC methodology. A) General scheme of CO_2 capture. Cations are not represented at scale for clarity. B) Sorption capacity with different hydroxide salts (*Sorption conditions:* 10 mL of hydroxide solution, 1 mol/L in H_2O, bubbling compressed air (75 mL/min), 25 ºC, 48 h). C) Quantitative ^{13}C NMR analysis of captured solutions (Na_2CO_3 using ethanol as internal standard).

Having successfully captured CO_2 into its active form TBA.HCO_3, the next objective was to design a catalyst capable of hydrogenating bicarbonate to formate salts to serve as feedstock in the biosynthesis of PHB. Catalytic activity, stability and the ease of separation and reutilisation in subsequent reaction cycles where the key design parameters. Hence, a series of Ru-N-heterocyclic carbenes (NHCs) organometallic complexes supported on macroporous polystyrene-divinylbenzene (PS-DVB) polymeric supports were synthesised, drawing inspiration from the Ru-MACHO-like shape catalyst, commonly used in literature.[21-23] A one-pot three-step reaction process (Figure S1-S6) was employed as a solid-phase synthetic strategy.[43] The structure of the resulting organometallic polymeric materials is illustrated in **Figure 3A**. These supported Ru-NHCs materials were chosen for their potential dual role. They can serve as chemical NHC–metal precursors for metal nanoparticles (MNPs) and act as potential surface ligands for MNPs due to their strong affinity for forming robust bonds with metals.[44] This dual functionality can control the generation of MNPs and enhance their effectiveness as catalytic systems by improving their stability, reactivity, and selectivity.[45] The formation of NHC complexes and their composition was characterised by different techniques (SI section S3-S6 and table S1). The Ru-NHC complexes C1 and C5 derived from

$[RuCl_2(CO)_2]_n$ exhibited a distinctive band at approximately 1565 cm^{-1}, corresponding to the C-N-C vibration of NHC (Figure S4). Additionally, the CO bands linked to the Ru-NHC complex appeared at 2046 cm^{-1} and 1969 cm^{-1}, and at 2048 cm^{-1} and 1973 cm^{-1}, for C1 and C5 respectively, confirming the formation of the Ru-NHC complexes. The XPS spectra also confirm their formation (**Figure 3B**, left). The catalyst C1 showed two superimposed peaks in the N1s area (see Figures S7). The peak at 399 eV corresponds to a carbenic nitrogen species, while the peak at 402 eV can be attributed to unreacted imidazolium species (Table S1).[46] Despite the strong overlap between the C 1s and Ru 3d spectra, it was also possible to identify the spin-orbit splitting of Ru $3d_5/_2$ and Ru $3d_3/_2$ at 282.1 eV and 286.3 eV, respectively. These peaks correspond to Ru^{3+}, likely in an octahedral geometry as expected for the Ru-NHC complex. Additionally, the Ru-Cl bond was observed, which is consistent with the expected complex (Figure S7).[47-49] Similar carbene/imidazolium ratios were also observed for C3 obtained employing $[RuCl_2(p\text{-}Cymene)_2]$ instead of $[RuCl_2(CO)_2]_n$ as metal precursors (Figure S8).

After the reaction, the carbon species remain unchanged for the compound C1 (**Figure 3B**, right). However, the Ru doublet exhibited a shift towards lower binding energy, with peaks centered at 281.2 eV and 285.4 eV, suggesting a change in its chemical environment, indicating an interaction between Ru and O (Ru-O) bonds. Additionally, the presence of two peaks centered at 462.5 eV and 485 eV, related to Ru $3p_3/_2$ and Ru $3p_1/_2$, respectively, clearly suggests the formation of RuO_2 nanoparticles after the reaction. This observation aligns well with previous literature research.[47-50]

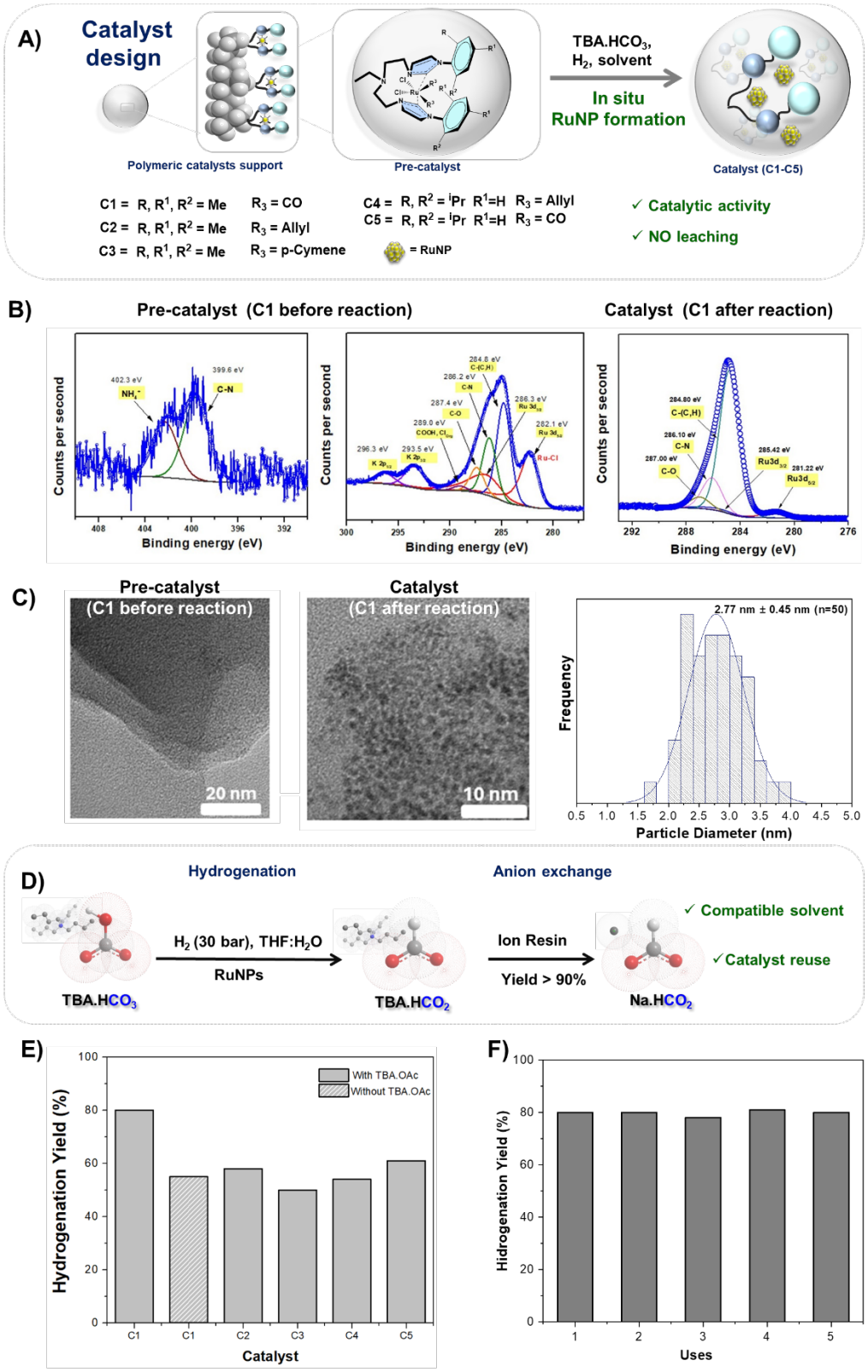

Figure 3. Formate generation. A) General scheme; C) XPS spectra at the N1s, C 1s + Ru 3d of C1 before and after reaction; C) TEM images of C1 before and after reaction and histogram of RuNPs size (see figures S10-S15); D) Scheme of the production of $NaHCO_2$. Cations are not drawn at scale for clarity. E) Hydrogenation reaction using different catalysts. F) Recycling

experiments of C1 catalyst. Reaction conditions: TBA.HCO_3 (1 mmol); TBA.OAc (0-0.5 mmol), 30 mg pre-catalyst, 30 bar H_2, 100 ^oC, THF: H_2O (1mL:1mL), 24h.

These systems underwent testing in the hydrogenation reaction of TBA.HCO_3 to produce TBA.formate (TBA.HCO_2) (**Figure 3D-3E**). Notably, C1 exhibited superior activity (78%) to the rest of catalysts. TEM images of this catalyst after the reaction revealed the in-situ formation of small and homogeneous Ru nanoparticles (RuNPs) with sizes of 2.77 nm ± 0.45 nm (**Figure 3C**). Other catalysts displayed larger particle sizes and occasional cluster formation (Figures S10-S15). The different results obtained confirm the importance of the electronic parameters and steric environment of the NHC ligands in leading to stable and active RuNP systems. These factors are crucial in optimizing the formation and performance of Ru nanoparticles, thereby enhancing the efficiency of the catalytic process. Indeed, when similar hydrogenation tests were conducted using either $[RuCl_2(CO)_2]_n$ or $RuCl_3$ as metal precursors absorbed onto the support ligand used for the preparation of C1 but without forming NHC complexes, a significant reduction in reaction activity was observed (Figure S16). Furthermore, this was accompanied by both metal leaching and the formation of larger nanoparticles (Figures S16-S17). These results underscore the importance of the Ru-NHC precursor in controlling the formation of RuNPs, stabilizing them to prevent aggregation and leaching, and thereby enhancing their catalytic efficiency.

A test evaluating catalyst reuse was conducted, revealing that the catalyst (C1) maintained consistent catalytic activity even after undergoing five reaction cycles (**Figure 3F,** Figure S9). The quantities of base and bicarbonate were adjusted to ensure equivalence with respect to the Ru equivalents present in the reaction, thus ensuring comparability across all cases. Additionally, the supernatant obtained after drying was analyzed to verify the presence of Ru. The results indicated a minimal degree of leaching (< 0.05% relative to Ru amount in the fresh catalyst). The results demonstrating the material's robustness and stability after multiple cycles under identical reaction conditions, thereby confirming the recyclability of Ru catalyst within the supported heterogeneous material.

It is noteworthy that C1 maintained good activity when used in the absence and presence of TBA acetate (TBA.OAc), achieving yields of 78% in the presence and 55% in its absence. This reduction in yield can be elucidated by the buffer effect exerted by TBA.OAc. This buffer shifts the equilibrium towards bicarbonate formation, thereby favouring the hydrogenation process towards formate production.[51-55] In the absence of this buffer salt, as formate starts to accumulate, the medium becomes more acidic, thereby shifting the equilibrium towards the formation of free CO_2, impeding further reaction progression. This methodology was chosen for scaling up production to a larger laboratory scale (10 mL tested) to generate pure formate solutions for the subsequent biocatalytic transformations. The

carbon source for formatotrophs and all possible impurities accompanying it should be compatible with the enzymes and microorganisms needed for microbial fermentation, both in terms of toxicity and osmoregulation. For these reasons, two different carbon sources were considered ($TBA.HCO_2$ and $NaHCO_2$) for their conversion into PHB. $NaHCO_2$ was easily obtained from $TBA.HCO_2$ through a cation exchange reaction using an ion exchange resin column, achieving a yield exceeding 90% without exhaustive optimization (**Figures 3D** and S19). In addition, the TBA was further reused to regenerate TBA.OH through an anion exchange resin, as detailed in the experimental procedure. It is important to highlight that this approach represents a closed-loop system, ensuring the complete recycling of the materials used. Once it was demonstrated that both sources of formic acid can be produced from CO_2 captured from the air, we focused on optimizing a bioprocess that employs them as the sole carbon and energy source for the growth and polyhydroxybutyrate (PHB) accumulation in *Cupriavidus necator* H16. This continuous bioprocess was optimized using Adaptive Laboratory Evolution (ALE).

Adaptive Laboratory Evolution

ALE experiments to maximimise the growth of *C. necator* H16 on formic acid with the aim of increasing the maximum growth rate (μ_{max}) of the organism were conducted (**Figure 4A**) The mass balance equations around biomass and growth-limiting substrate in a continuous (chemostat) fermentation were calculated. The direct link between the dilution rate (D) and the growth rate (μ) renders the chemostat a great tool to target growth rate as the optimisation target for ALE campaigns.

In this study, *C. necator* H16 was subjected to continuous fermentation over almost five months with stepwise increasing dilution rates. In prior batch fermentations, the maximum growth rate of the strain in 1 L batch cultivations on 80 mM free formic acid as the sole carbon source was determined as $0.14 \pm 0.01\ h^{-1}$ (Figure S20). Throughout the chemostat fermentation, biomass levels were stable over the varying dilution rates and no residual formic acid was detected in the reactor (**Figure 4B**, online data shown in Figure S21). As a general trend, after the initial establishing of the chemostat it could be observed that biomass increased with the increase in the dilution rate. To test formic acid tolerance of the bacterium, the respective concentration was doubled temporarily after 129 days resulting in a spike in biomass. It normalised again after reverting to the desired 80 mM formic acid in the feed, demonstrating the stability of the process. The highest dilution rate used in the ALE experiment was $0.16\ h^{-1}$ after which the evolution campaign was terminated.

Screening of ALE Variants

From an endpoint sample taken from the ALE experiment, 42 isolated single colonies were selected randomly for growth screening in a BioLector I against a triplicate culture of the wildtype (WT) strain. The μ_{max} of each strain was determined and compared to that of the WT triplicate (**Figure 4C**). The five best performing colonies (*C. necator* ALE14, *C. necator* ALE25, *C. necator* ALE26, *C. necator* ALE31, *C. necator* ALE38) were subsequently analysed in shake flask cultures.

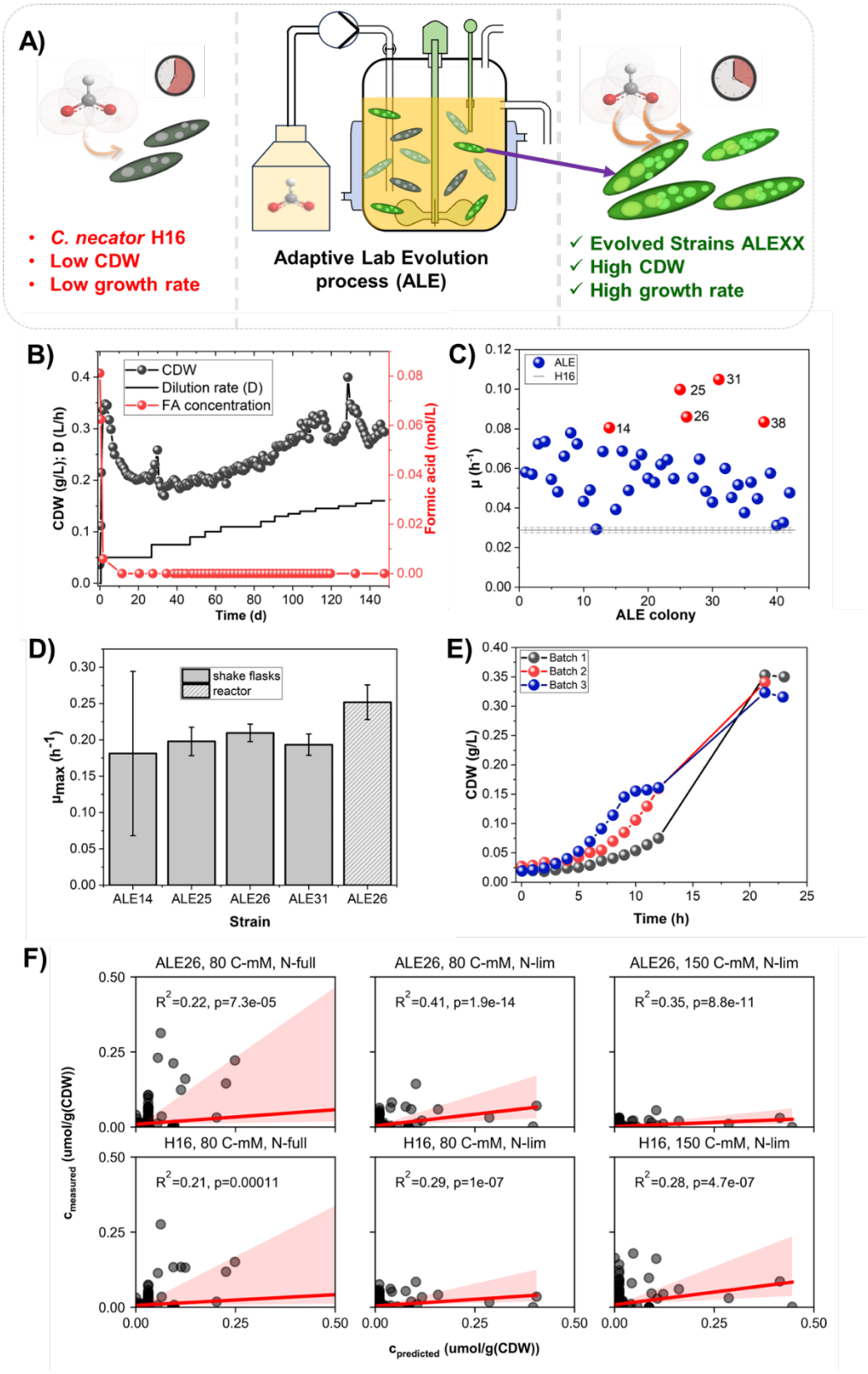

Figure 4. ALE procedure and screening. A) Schematic overview of the aim of the ALE campaign. B) Offline biomass determination (cell dry weight (CDW)), residual formic acid measurement and dilution rate over the course of the evolution campaign. C) Maximum growth rates of 42 randomly selected colonies isolated from the final time point of the ALE campaign

alongside a triplicate of *C. necator* H16. D) μ_{max} of the best performing ALE strains and of *C. necator* ALE26 in batch fermentations in a bioreactor. E) Batch fermentations of *C. necator* ALE26 over 22 h on 80 mM formic acid as the sole carbon source. F) Correlation of measured and resource balance analysis (RBA)-predicted protein expression for each tested growth condition and strain (*C. necator* ALE26 in the first row, *C. necator* H16 in the second).

Growth profiles of *C. necator* ALE25, ALE26 and ALE31 in flasks (Figure S22) were very similar whilst precultures for ALE38 did not grow and ALE14 showed long lag phases. The observed maximum growth rates are shown in **Figure 4D**. *C. necator* ALE26 was selected for further experiments. When grown in a 1 L batch fermentation, growth profiles of *C. necator* ALE26 differed slightly across repeats (**Figure 4E**). However, final biomass titres and maximal observed growth rates across repeats are very similar (**Figure 4D**). The observed μ_{max} for *C. necator* ALE26 on 80 mM formic acid was 0.25 ± 0.02 h^{-1}, signifying a 1.8-fold increase compared to what was observed for the WT strain in this study and a 1.4-fold improvement compared the literature.[29]

Strain Characterisation

Genome sequencing of *C.necator* ALE26 and comparison with the genome of the WT strain revealed that the main difference between the strains originated from the absence of the megaplasmid pHG1 in the evolved strain (See SI, section S10 and Figure S23).

This pHG1-loss is interestingly parallel to the findings by Calvey *et al.,* although here a full loss of the plasmid was found whereas their study reported large partial deletions.[56] The rationalisation for the deletions given in their work holds true in this case as well. While pHG1 harbours a second copy of the CBB operon, otherwise also present on chromosome 2, this second copy lacks the LysR-type transcriptional regulator gene *cbbR*.[57] Other genetic elements responsible for hydrogen metabolism, degradation of aromatic compounds and plasmid maintenance and transmission do not play a vital role in the cultivation conditions applied,[58] although many of the respective genes have been shown to be constitutively expressed across several growth conditions, even in those where they do not seem to have an active metabolic role.[59, 60] Both strains exhibit very similar maximum growth rates on formic acid despite the different approaches to the laboratory evolution. Strikingly however, the highest growth rate documented in their work (0.245 ± 0.011 h^{-1}) was observed for a deletion mutant of the transcriptional regulator PhcA (Δ*phcA*). The gene in their adapted strain was disrupted by a frameshift mutation and was identified as the major contributor to the improved growth rates alongside the (partial) deletion of pHG1. This gene corresponds to the locus

E6A55_00465 in the genome sequence used for reference in this work.[61] The same mutation could not be observed in this study, where the gene appears to be undisrupted.

For further functional analysis of the newly evolved strain, both it and the WT strain were grown in continuous culture under three different growth conditions: on 80 mM formic acid at a carbon/nitrogen ratio (C/N ratio, [mol/mol]) of (i) 5.3 mol/mol or (ii) 50 mol/mol as well as (iii) 150 mM formic acid at C/N = 50 mol/mol, all at a dilution rate of 0.09 h^{-1}. In every condition, a large number of proteins were observed only in one of the two strains (Figure S24). Many of these proteins correlate with proteins found on pHG1, yet there are additional chromosomal genes that only see functional expression in one or the other organism. Regulatory shifts across cellular processes like quorum sensing, for which annotated proteins appear to be consistently upregulated across growth conditions, indicate a wide-ranging reorganisation of gene expression in the evolved strain.

To analyse general trends of proteome utilisation between the strains, resource balance analysis (RBA) was employed.[62, 63] In the mathematical model, the metabolic cost associated with protein expression is minimised by reducing expression to a minimum necessary to support that growth rate. Our hypothesis was that if *C. necator* ALE26 outperforms the WT strain in terms of growth, that the improved growth rate of *C. necator* ALE26 should be reflected to some extent in the allocation of resources, i.e. protein expression. Therefore, the proteome profile of the strain should correlate more closely with an optimised prediction provided by the RBA module. Proteomic prediction was performed for proteins contained in the model as well as in the proteomic data sets, predicted and measured levels were than correlated and the squared Pearson correlation coefficient calculated (**Figure 4F**).[59] For each tested growth condition, the correlation is higher for the evolved strain than for the WT strain, indicating a protein distribution closer to a predicted optimum. Notably, this correlation is greatest for the growth condition on 80 mM formic acid and in nitrogen limiting (*i.e.* PHB accumulating) conditions. Here, the overall nutrient availability is the lowest out of the three tested conditions (low carbon and nitrogen), leading to the predicted μ_{max} being the closest to the actual growth rate (as determined by the dilution rate). This feeds into our hypothesis of resource conservation following a deletion of unnecessarily expressed genes (in the form of pHG1) enabling the increased growth. While the strain presented here shows a similar growth rate to the Δ*phcA*-strain mentioned above without the loss or disruption of the eponymous gene, it should be noted that the growth rate determined by Calvey *et al.* was taken from a flask experiment. The one demonstrated here stems from a fermentation in a stirred tank reactor. Growth rates tend to be higher in these more controlled systems. Therefore, a genomic deletion of the transcriptional regulator might further enhance growth performance of *C. necator* ALE26 in bioreactors.

Polyhydroxybutyrate Production

The accumulation of PHB in a continuous fermentation was optimised with *C. necator* ALE26 in a biotechnological context (**Figure 5A**). The parameters optimised in a continuous fermentation were C/N ratio, dilution rate and absolute carbon concentration. Growth profiles for fermentations altering these parameters can be found in the supplementary information (Figures S25-S27 and Figure S28 for cultivation of *C. necator* H16).

C/N ratios of 25 mol/mol and lower resulted in a very low PHB content (**Figure 5A**). A C/N ratio of 50 mol/mol and higher resulted in bacterial cells accumulating approximately 15 % of CDW as PHB, with higher C/N ratios showing similar PHB contents. Nevertheless, the maximum space time yield (STY) was achieved at 50 mol/mol with a drop in productivity at higher ratios. This correlates with a higher total biomass at lower C/N ratios (Figure S30). A low C/N ratio showing the best productivity falls in line with experiments that have shown that the ratio between carbon and the growth-limiting nutrient is not arbitrary as a minimal residual nutrient concentration is required for cellular maintenance processes.[64-66]

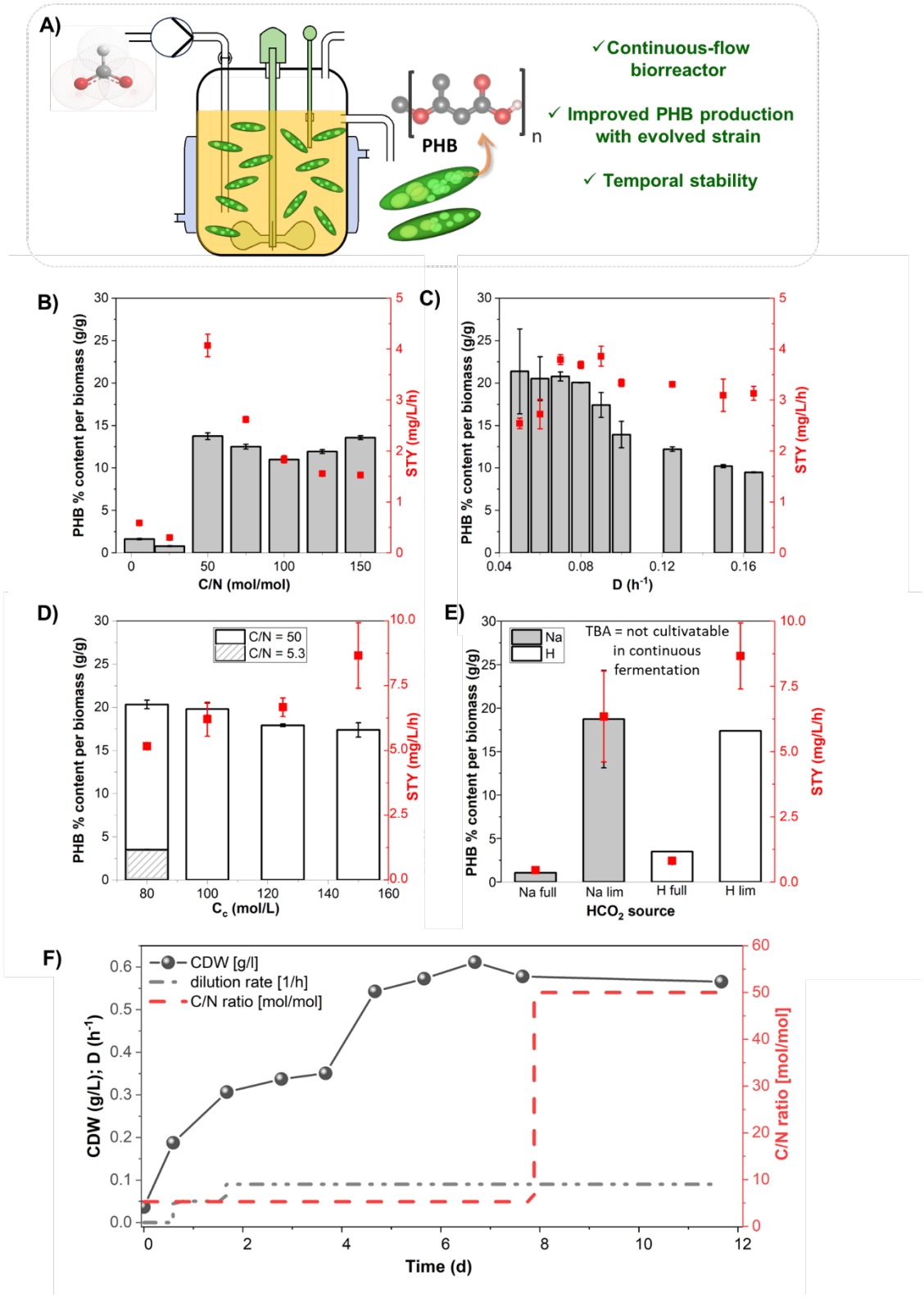

Figure 5. Optimisation of PHB accumulation and growth of *C. necator* ALE26 in a continuous fermentation. A) Principle of the production of PHB in a continuous fermentation system from formate salt and formic acid. B) PHB content (gPHB/gCDW) and STY across varying C/N ratios at D = 0.1 h^{-1} and 80 mM formic acid in the feed medium. C) PHB content and STY across varying dilution rates at C/N = 50 mol/mol and 80 mM formic acid in the feed medium.

D) PHB content and STY across varying formic acid concentrations in the feed at C/N = 50 mol/mol and D = 0.09 h^{-1}. E) Comparison of PHB production depending on sodium formate or free formic acid as the carbon source. F) Biomass data and process parameters for continuous cultivation on sodium formate of *C. necator* ALE26.

The results from varying the dilution rate suggest a decreasing trend in PHB accumulation with increasing dilution rates, as the percentage of PHB of the CDW dropped from around 21.37 ± 4.99 % at 0.050 h^{-1} to 9.47 ± 0.05 % at 0.165 h^{-1} (**Figure 5C**). However, when factoring in the time component via the dilution rate it became apparent that the STY did not change drastically for dilution rates between 0.07 h^{-1} and 0.165 h^{-1}, reaching its maximum at 3.9 ± 0.2 mg L^{-1} h^{-1} at D = 0.09 h^{-1}. This follows the proposed partial coupling between growth- and PHB accumulation rate by Grousseau et al.[65] which explains why the chemostat is ideally performed at medium dilution rates rather than close to the μ_{max} of the organism.

Higher formic acid concentration did not correlate with a higher PHB content per cell (**Figure 5D**). In fact, the PHB content dropped slightly at the higher substrate concentrations. Overall, the PHB content of *C. necator* ALE26 was significantly higher than in the WT strain, reaching up to 20.3 ± 0.5 % (Figure S29). However, the productivity (STY) in both cases increased with higher formic acid concentrations as the active biomass increased. Again, the evolved strain outperformed the WT strain with a maximum productivity of 8.67 ± 1.26 mg L^{-1} h^{-1} at a formic acid feed concentration of 150 mM. This translates to a carbon yield of 0.03 mol(C_{PHB})/mol($C_{formic\ acid}$).

The conservation of resources from losing pHG1, as discussed earlier, could also explain the discrepancy seen in PHB accumulation between *C. necator* H16 and ALE26 (Figure S29). As less nutrients need to be dedicated to protein expression or cell division, more can be allocated towards carbon storage in the adapted strain. It has been shown before that under PHA producing conditions the cellular composition changes, with proportionally less protein expression during nutrient limitation[64] which reflects the shifting of resources necessary to accumulate the polymer. This shift might be made easier by the lack of the additional metabolic burden exhibited by the megaplasmid.

Overall, the STY of PHB from formic acid achieved in this work is on par or surpasses those documented so far whilst being more robust over time than a fed-batch fermentation.[35, 36, 39] The comparatively low polymer yields might be improved with further process optimisation and more complex setups such as multiphase fermentations and medium recirculation methods.

Conversion of atmospheric CO_2 into PHP via formate to bridge air-capturing CO_2 to producing PHB, the primary product, TBA.HCO_2, was tested for growth of *C. necator* ALE26 in the BioLector. The organism was cultivated on varying concentrations of TBA. HCO_2 as the sole carbon source as well as free formic acid and sodium gluconate supplemented with TBA. HCO_2 in varying concentrations (Figure S30). Growth was observed for conditions in which TBA.HCO_2 was the sole carbon source as well as when it was added with formic acid or sodium gluconate, albeit at very slow rates.

While *C. necator* ALE26 grew on low concentrations of TBA. HCO_2 and accumulated up to 29.51 % (g_{PHB} g_{CDW}^{-1}) in shake flasks (Figure S31), its growth rate was too low to permit growth in continuous fermentations. With the development of the ion-exchange method to convert TBA.HCO_2 into sodium formate, the latter can be used for a continuous fermentation whilst avoiding the toxicity of the TBA cation. The overall productivity of PHB on sodium formate was similar to that of the free acid (**Figure 5E**). Thus, a fermentation was carried out on 160 mM sodium formate as the sole carbon source and with optimised conditions for PHB accumulation (D = 0.09 h^{-1} and C/N = 50 mol/mol, **Figure 5F**). Samples for PHB measurement were taken in full and nitrogen-limited conditions for comparison with the growth on free formic acid. A final PHB content of 18.73 ± 5.59 % was achieved, giving a STY of 6.34 ± 1.75 mg L^{-1} h^{-1} (**Figure 5E**).

The synthesis of PHB from CO_2 waste streams is the subject of numerous studies, but use of CO_2 or CO_2-derived compounds as primary reactants remains relatively uncommon. **Table S6** highlights the most relevant studies where pure CO_2, or CO_2 from flue gas has been employed in the production of PHB under diverse biological conditions. In phototrophic processes with flue gas containing 3-6% of CO_2, STYs of maximum 3.02 mg L^{-1} h^{-1} have been reported (entries 1- 2).[38, 67] The highest productivity to date described for PHB accumulation from CO_2-derived formate was found in a two-stage system employing non-growing C necator H16 cells in a biotransformation (entry 3).[39] With this system, Dinges *et al.* achieved up to 8.4 mg L^{-1} h^{-1} (per OD_{600}). However, while their experiments gave valuable insights into theoretical PHB yields from formate, biotransformations such as the one described generally become unstable over time due to cell lysis or enzyme degradation. While lower than those reported for pure CO_2 as the carbon source (up to 12.54 mg L^{-1} h^{-1}),[68, 69] those studies using diluted sources of CO_2 demonstrate that these waste gases may still be usable as a direct feedstock for polymer accumulation.

Our results, where CO_2 was directly captured from the air (0.04% of CO_2), show that the PHB STY (6.34 ± 1.75 mg L^{-1} h^{-1}, entry 4) is comparable to results where diluted CO_2 or formate was utilized. At the same time, to the best of the author's knowledge this is the first

time a continuous fermentation for accumulation of PHB from formate has been described, which can be run for long periods of time without the risk of instabilities or the requirement for repeated stopping and starting of the process. This underscores the potential of our integrated biochemical and catalytic process to efficiently produce PHB, a chemical of significant industrial interest.

Conclusion

This study is a proof-of-concept of a chemo-biocatalytic process to upcycle captured atmospheric CO_2 via formate salts to polyhydroxybutyrate. The direct capture process employing ionic liquids under aqueous conditions, and novel immobilised nanostructured catalysts, represents a simple, yet efficient means that will open up new possibilities for transforming CO_2 into valuable products. This non-conventional feedstock was employed to produce a biodegradable polymer polyhydroxybutyrate. This process integrates CO_2 capture and polypropylene-like polymer production completely decoupled from fossil-feedstock, and the end product opens multiple applications and new end-of-life management options. The power of adaptive laboratory evolution to yield a strain with improved growth rate due to the optimised resource efficiency, coupled with bioprocess development showcased here can also serve as basis to further exploit existing microbial biocatalysts' anabolic reactions, or metabolism extended by new-to-nature synthesis pathways to produce a plethora of valuable products.

This first proof of concept of an interdisciplinary pipeline for atmospheric CO_2 fixation and utilisation to generate biodegradable polymers (**Figure 6**), will inspire new avenues to simultaneously help tackling climate change and generate circular economy approaches for the plastic industry.

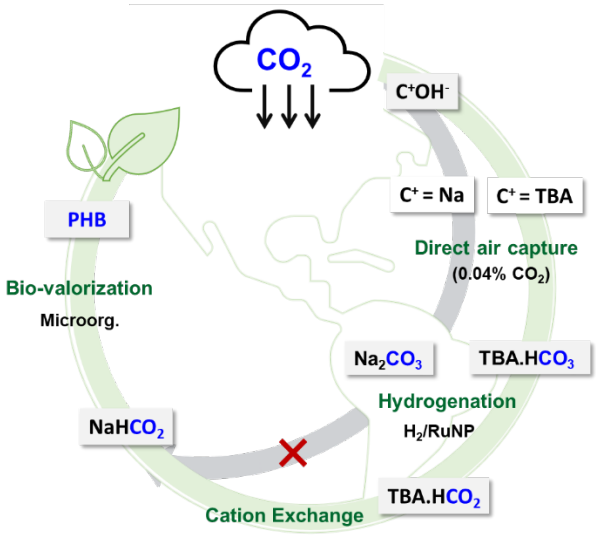

Figure 6. Schematic representation of a pipeline for atmospheric CO_2 capture and transformation in biodegradable polymers.

Experimental

Direct air capture

The samples for CO_2 capture were prepared using a solution of 1 mol/L of TBA.OH in H_2O (0.5-100 mL) The sorption experiments were performed by bubbling the gas (compressed air) in a vial glass tubes with a septum at 25 ^oC for 48h.[42] For the CO_2 sorption quantification, we have previously established this NMR methodology for CO_2 quantification in ILs.[70, 71] Typically, ^{13}C NMR inverse gated ^1H decoupled spectra were acquired using an inversion recovery experiment (zgig) with a relaxation delay of 60 seconds. The experiments were performed with 64 transients with 64K data points were collected.

Catalyst preparation

$Ru(CO)_2Cl_2$ was synthesised according to a previously reported method (see section S3 at the SI).[72]

Hydrogenation reaction

Catalytic reactions were performed in a stainless-steel batch reactor of 30 mL with a pressure regulator. Typically, 1 mmol of $TBA.HCO_3$, 0.5 mmol of TBA.OAc and a mixture of solvent (in almost all of the cases 1:1 of water/THF) were put together along with the desired amount of catalyst. Then, the reactor was fully pressured at 5, 30 or 50 H_2 bar based on each specific condition. Initially, the reactions were carried out at 100°C, however, in some cases, the effect of temperature was also studied. Quantification of the amount of formate (yield) was performed with ^1H NMR with the signal at ~8.3 ppm and referenced with the signals of TBA cation at ~0.8 ppm (18 protons) (see Figure S18-S19 in supporting information). For the reuse, the catalyst was removed from the reaction mixture by centrifugation and the residual was washed with dichloromethane and methanol (3x10 mL) and dried overnight at 50°C (vacuum). The liquid phase was separated to further cation exchange. The remaining catalyst was analyzed by using ICP-MS to estimate the Ru amount (in ppm). The catalyst was also tested as used without any pretreatment and the results were compared with the material washed and dried.

Cation and anion exchange procedure

The cation exchange from $TBA.HCO_2$ to $NaHCO_2$ was conducted using an ion exchange resin (Amberlite IR-120 in H+ form). Aqueous TBA. HCO_2 solution (1 M) was gradually passed through a resin-filled column. The eluate was then collected in a vial

containing an equimolar amount of NaOH solution, resulting in the formation of Na HCO_2. The solvent was evaporated under reduced pressure using a rotary evaporator and dried for 8 hours at 60°C under vacuum. The TBA was further reused to produce TBA.OH a Amberlyst A26 (OH^- form), according to previous describe procedure.[42]

Cultivation in Bioreactors

All bioreactor cultivations were carried out in stirred tank vessels of the F0-Baby model by Bionet (Fuente Álamo (Murcia), Spain) at a working volume of 1 L. The process was controlled and monitored using the company's ROSITA software.

Batch Cultivations

Fermentations were carried out using J-minimal medium (J-MM) (supplementary materials, S2.3).[73] Precultures were grown in shake flasks (supplementary materials, S2.4), the last of which took place in 100 mL J-MM in 1 L baffled shake flasks. The reactor was inoculated from this to a starting OD_{600} of 0.05. The initial stirrer speed was set to 500 rpm and gas flow to 1 L_{gas} L_{liquid}^{-1} min^{-1}. Dissolved oxygen (DO) in the vessel was regulated at a minimum of 20 % by an increase of stirring speed followed by an increase in air flow up to 1500 rpm and 3 L_{gas} L_{liquid}^{-1} min^{-1}respectively. pH was controlled at 7.2 by feeding 4 M KOH and 15 % (v/v) H_2SO_4. Furthermore, CO_2 and O_2 content in the exhausted air were analysed via a Breath module from Bionet. Samples were taken in regular intervals to be analysed for biomass content and carbon and nitrogen concentration estimation. More details are given in the supplementary materials, S2.5.1.

Continuous Cultivation

For continuous cultivations, the bioreactor was set up as described in the supplementary materials, S2.5. It was operated in batch for 12 h before the pumps were activated. The feed was controlled manually by setting the pump rate to match the desired dilution rate [h^{-1}]. Spent medium (bleed) was harvested by controlling the weight of the bioreactor using a Defender™ 5000 scale (Ohaus, Parsippany, NJ, USA) so that over time it would remain constant despite the continuous feed and pH control. The fed medium was J-MM, with concentrations of the desired carbon source and $(NH_4)_2SO_4$ matching the conditions desired in each experiment. Samples were taken directly from the bioreactor rather than from the bleed line with the weight-controlled bleed ensuring that the full volume would fill up in a temporary fed-batch process before re-entering true continuous operation.

Cultivation in a BioLector

For condition testing and screening, *C. necator* was cultivated in a BioLector 1 (Beckman Coulter, Brea, California, USA). Cultivations were performed in 1 mL total culture volume in

48-well flower plates with oxygen and pH sensors (MTP-48-BOH 1, Beckman Coulter). Temperature in the incubation chamber was controlled at 30 °C, humidity at 70 – 80 % and shaking was set to 1000 rpm. The plate was inoculated from two-step 3 mL J-MM precultures, similar to the preparation for Cultivation in Baffled Shake Flasks. Cultivations were performed in J-MM with the required amounts of carbon and nitrogen added for each experiment. Blanks were run in triplicates of uninoculated medium. The ALE experiment and subsequent screening are described in the supplementary information in sections S2.5 and S2.6 - S2.9. Analytical procedures accompanying the fermentations are described in the supplementary information in section S2.10

Proteomics analysis

For proteomics analysis of *C. necator* strains under different growth conditions, biological duplicate samples were collected and further split into two technical replicates each (sample preparation is detailed in the supplementary materials, S2.11.1). Samples were handed to the Proteomics Core facilities of University College Dublin. There, samples were run in a Thermo Scientific Q Exactive workflow with the Thermo Scientific Ultimate 3000 RSLCnano chromatography system (electrospray ionisation liquid chromatography-mass spectrometry (ESI LC-MS), using a quadrupole with high resolution high mass accuracy (HRAM) by Orbitrap). Peaks were analysed in these facilities using MaxQuant software. Data analysis and statistics were performed in Perseus (Max Planck Institute of Biochemistry, München, Germany), GraphPad PRISM and python, as outlined in the supplementary materials, S2.11.2 and S2.11.3.

ACKNOWLEDGMENTS

This work was supported by the projects (PID2021-124695OB-C22), MICINN/AEI/10.13039/501100011033 and by (TED2021-130288B-I00) funded by MCIN/AEI/10.13039/501100011033 and the Unión Europea NextGenerationEU/ PRTR. Generalitat Valenciana is gratefully acknowledged for funding for GenT (CIDEGENT 2018/036). The project that gave rise to these results received the support of a fellowship LCF/BQ/PR24/12050016 from the “la Caixa” Foundation (ID 100010434). This work was further supported by Science Foundation Ireland BiOrbic research centre (SFI reference number: 16/RC/3889) through the Centre for Doctoral Training Atoms-to-Products - an Integrated Approach to Sustainable Chemistry (BiOrbic) under the grant number 18/EPSRC-CDT/3582. TN is a recipient of Ad Astra Fellowship at UCD. The authors acknowledge the Ministry of Education, Youth and Sports of the Czech Republic, for the financial support of XPS measurements using the CEMNAT infrastructure (project LM 2023037).

CONFLICTS OF INTEREST

There are no conflicts to declare.

Author Contributions: VS, KO, MZ, TN - Conceptualisation; MB, JESV, EGV - Methodology; MB, NP - Software Programming; MB, MZ, JESV and JRP - Investigation; MB, JESV, MZ Writing - Original Draft; all authors Writing - Review & Editing; MZ, VS, KO, TN, EGV - Supervision; MZ, VS, KO, EGV - Project administration; MZ, VS, EGV, KO - Funding acquisition.

References

1. IPCC, *Climate Change 2021: The Physical Science Basis. Contribution of Working Group I to the Sixth Assessment Report of the Intergovernmental Panel on Climate Change*, 2021.

2. IPCC, *Climate Change 2022: Impacts, Adaptation and Vulnerability. Contribution of Working Group II to the Sixth Assessment Report of the Intergovernmental Panel on Climate Change*, 2022.

3. IPCC, *Climate Change 2022: Mitigation of Climate Change. Contribution of Working Group III to the Sixth Assessment Report of the Intergovernmental Panel on Climate Change*, 2022.

4. G. Althor, J. E. M. Watson and R. A. Fuller, *Scientific Reports*, 2016, **6**, 20281.

5. P. Friedlingstein, M. O'Sullivan, M. W. Jones, R. M. Andrew, L. Gregor, J. Hauck, C. Le Quéré, I. T. Luijkx, A. Olsen, G. P. Peters, W. Peters, J. Pongratz, C. Schwingshackl, S. Sitch, J. G. Canadell, P. Ciais, R. B. Jackson, S. R. Alin, R. Alkama, A. Arneth, V. K. Arora, N. R. Bates, M. Becker, N. Bellouin, H. C. Bittig, L. Bopp, F. Chevallier, L. P. Chini, M. Cronin, W. Evans, S. Falk, R. A. Feely, T. Gasser, M. Gehlen, T. Gkritzalis, L. Gloege, G. Grassi, N. Gruber, Ö. Gürses, I. Harris, M. Hefner, R. A. Houghton, G. C. Hurtt, Y. Iida, T. Ilyina, A. K. Jain, A. Jersild, K. Kadono, E. Kato, D. Kennedy, K. Klein Goldewijk, J. Knauer, J. I. Korsbakken, P. Landschützer, N. Lefèvre, K. Lindsay, J. Liu, Z. Liu, G. Marland, N. Mayot, M. J. McGrath, N. Metzl, N. M. Monacci, D. R. Munro, S. I. Nakaoka, Y. Niwa, K. O'Brien, T. Ono, P. I. Palmer, N. Pan, D. Pierrot, K. Pocock, B. Poulter, L. Resplandy, E. Robertson, C. Rödenbeck, C. Rodriguez, T. M. Rosan, J. Schwinger, R. Séférian, J. D. Shutler, I. Skjelvan, T. Steinhoff, Q. Sun, A. J. Sutton, C. Sweeney, S. Takao, T. Tanhua, P. P. Tans, X. Tian, H. Tian, B. Tilbrook, H. Tsujino, F. Tubiello, G. R. van der Werf, A. P. Walker, R. Wanninkhof, C. Whitehead, A. Willstrand Wranne, R. Wright, W. Yuan, C. Yue, X. Yue, S. Zaehle, J. Zeng and B. Zheng, *Earth Syst. Sci. Data*, 2022, **14**, 4811-4900.

6. T. M. Gür, *Progress in Energy and Combustion Science*, 2022, **89**, 100965.

7. H. Li, M. E. Zick, T. Trisukhon, M. Signorile, X. Liu, H. Eastmond, S. Sharma, T. L. Spreng, J. Taylor, J. W. Gittins, C. Farrow, S. A. Lim, V. Crocellà, P. J. Milner and A. C. Forse, *Nature*, 2024, DOI: 10.1038/s41586-024-07449-2.

8. M. Zanatta, *ACS Materials Au*, 2023, **3**, 576-583.

9. A. Weilhard, S. P. Argent and V. Sans, *Nature Communications*, 2021, **12**, 231.

10. S. Moret, P. J. Dyson and G. Laurenczy, *Nature Communications*, 2014, **5**, 4017.

11. E. González, C. Marchant, C. Sepúlveda, R. García, I. T. Ghampson, N. Escalona and J. L. García-Fierro, *Applied Catalysis B: Environmental*, 2018, **224**, 368-375.

12. A. Bahuguna and Y. Sasson, *ChemSusChem*, 2021, **14**, 1258-1283.

13. C. Hao, S. Wang, M. Li, L. Kang and X. Ma, *Catalysis Today*, 2011, **160**, 184-190.

14. X. Meng, Z. Ju, S. Zhang, X. Liang, N. Von Solms, X. Zhang and X. Zhang, *Green Chemistry*, 2019, **21**, 3456-3463.

15. W. Hui, X. Wang, X.-N. Li, H.-J. Wang, X.-M. He and X.-Y. Xu, *New Journal of Chemistry*, 2021, **45**, 10741-10748.

16. J. Kothandaraman, A. Goeppert, M. Czaun, G. A. Olah and G. K. S. Prakash, *Journal of the American Chemical Society*, 2016, **138**, 778-781.

17. R. Sen, A. Goeppert, S. Kar and G. K. S. Prakash, *Journal of the American Chemical Society*, 2020, **142**, 4544-4549.

18. R. Sen, C. J. Koch, V. Galvan, N. Entesari, A. Goeppert and G. K. S. Prakash, *Journal of CO2 Utilization*, 2021, **54**, 101762.

19. S. Kar, A. Goeppert and G. K. S. Prakash, *ChemSusChem*, 2019, **12**, 3172-3177.

20. D. Mellmann, P. Sponholz, H. Junge and M. Beller, *Chemical Society Reviews*, 2016, **45**, 3954-3988.

21. R. Bhardwaj, A. Kumar and J. Choudhury, *Chemical Communications*, 2022, **58**, 11531-11534.

22. D. Wei, H. Junge and M. Beller, *Chemical Science*, 2021, **12**, 6020-6024.

23. C. Guan, Y. Pan, E. P. L. Ang, J. Hu, C. Yao, M.-H. Huang, H. Li, Z. Lai and K.-W. Huang, *Green Chemistry*, 2018, **20**, 4201-4205.

24. A. B. Hooper and A. A. DiSpirito, in *Encyclopedia of Biological Chemistry (Second Edition)*, eds. W. J. Lennarz and M. D. Lane, Academic Press, Waltham, 2013, DOI: https://doi.org/10.1016/B978-0-12-378630-2.00219-X, pp. 486-492.

25. H. Salehizadeh, N. Yan and R. Farnood, *Chemical Engineering Journal*, 2020, **390**, 124584.

26. N. S. Kruyer and P. Peralta-Yahya, *Biochemistry*, 2020, **59**, 731-732.

27. F. Joó, *ChemSusChem*, 2008, **1**, 805-808.

28. S. Farzani Tolesorkhi, F. Esmaeilzadeh and M. Riazi, *Petroleum Research*, 2018, **3**, 370-380.

29. S. Grunwald, A. Mottet, E. Grousseau, J. K. Plassmeier, M. K. Popović, J.-L. Uribelarrea, N. Gorret, S. E. Guillouet and A. Sinskey, *Microb Biotechnol*, 2015, **8**, 155-163.

30. M. Beeby, M. Cho, J. Stubbe and G. J. Jensen, *Journal of Bacteriology*, 2012, **194**, 1092-1099.

31. L. Garcia-Gonzalez, M. S. I. Mozumder, M. Dubreuil, E. I. P. Volcke and H. De Wever, *Catalysis Today*, 2015, **257**, 237-245.

32. H. G. Schlegel, R. Lafferty and I. Krauss, *Archiv fur Mikrobiologie*, 1970, **71**, 283-294.

33. A. Steinbüchel and B. Füchtenbusch, *Trends in biotechnology*, 1998, **16**, 419-427.

34. J. Lu, C. J. Brigham, S. Li and A. J. Sinskey, in *Biotechnology for Biofuel Production and Optimization*, eds. C. A. Eckert and C. T. Trinh, Elsevier, Amsterdam, 2016, DOI: https://doi.org/10.1016/B978-0-444-63475-7.00012-1, ch. 12, pp. 325-351.

35. R. Tang, C. Weng, X. Peng and Y. Han, *Metabolic Engineering*, 2020, **61**, 11-23.

36. S. Kim, Y. J. Jang, G. Gong, S.-M. Lee, Y. Um, K. H. Kim and J. K. Ko, *Microbial Cell Factories*, 2022, **21**, 231.

37. A. Satanowski and A. Bar-Even, *EMBO reports*, 2020, **n/a**, e50273.

38. A. Langsdorf, J. P. Schütz, R. Ulber, M. Stöckl and D. Holtmann, *Journal of CO2 Utilization*, 2024, **83**, 102800.

39. I. Dinges, I. Depentori, L. Gans, D. Holtmann, S. R. Waldvogel and M. Stöckl, *ChemSusChem*, 2024, **17**, e202301721.

40. K. Müller, K. Brooks and T. Autrey, *Energy & Fuels*, 2017, **31**, 12603-12611.

41. D. J. Heldebrant, J. Kothandaraman, N. M. Dowell and L. Brickett, *Chemical Science*, 2022, **13**, 6445-6456.

42. M. Zanatta, E. García-Verdugo and V. Sans, *ACS Sustainable Chemistry & Engineering*, 2023, **11**, 9613-9619.

43. V. Sans, F. Gelat, M. I. Burguete, E. Garcia-Verdugo and S. V. Luis, *Catalysis Today*, 2012, **196**, 137-147.

44. M. Ghosh and S. Khan, *ACS Catalysis*, 2023, **13**, 9313-9325.

45. M. Koy, P. Bellotti, M. Das and F. Glorius, *Nature Catalysis*, 2021, **4**, 352-363.

46. A. Palazzolo, T. Naret, M. Daniel-Bertrand, D.-A. Buisson, S. Tricard, P. Lesot, Y. Coppel, B. Chaudret, S. Feuillastre and G. Pieters, *Angewandte Chemie International Edition*, 2020, **59**, 20879-20884.

47. S. M. Thalluri, J. Rodriguez-Pereira, R. Zazpe, B. Bawab, E. Kolíbalová, L. Jelinek and J. M. Macak, *Small*, 2023, **19**, 2300974.

48. H. Wang, X. Li, Q. Ruan and J. Tang, *Nanoscale*, 2020, **12**, 12329-12335.

49. A. F. Pedersen, M. Escudero-Escribano, B. Sebok, A. Bodin, E. Paoli, R. Frydendal, D. Friebel, I. E. L. Stephens, J. Rossmeisl, I. Chorkendorff and A. Nilsson, *The Journal of Physical Chemistry B*, 2018, **122**, 878-887.

50. M. Lin, L.-X. Dai, J. Gu, L.-Q. Kang, Y.-H. Wang, R. Si, Z.-Q. Zhao, W.-C. Liu, X. Fu, L.-D. Sun, Y.-W. Zhang and C.-H. Yan, *RSC Advances*, 2017, **7**, 33078-33085.

51. A. Weilhard, M. I. Qadir, V. Sans and J. Dupont, *ACS Catalysis*, 2018, **8**, 1628-1634.

52. L. Piccirilli, B. Rabell, R. Padilla, A. Riisager, S. Das and M. Nielsen, *Journal of the American Chemical Society*, 2023, **145**, 5655-5663.

53. W. D. G. Gonçalves, M. Zanatta, N. M. Simon, L. M. Rutzen, D. A. Walsh and J. Dupont, *ChemSusChem*, 2019, **12**, 4170-4175.

54. N. M. Simon, M. Zanatta, F. P. dos Santos, M. C. Corvo, E. J. Cabrita and J. Dupont, *ChemSusChem*, 2017, **10**, 4927-4933.

55. Y. Yasaka, C. Wakai, N. Matubayasi and M. Nakahara, *The Journal of Physical Chemistry A*, 2010, **114**, 3510-3515.

56. C. H. Calvey, V. Sànchez i Nogué, A. M. White, C. M. Kneucker, S. P. Woodworth, H. M. Alt, C. A. Eckert and C. W. Johnson, *Metabolic Engineering*, 2023, **75**, 78-90.

57. A. Pohlmann, W. F. Fricke, F. Reinecke, B. Kusian, H. Liesegang, R. Cramm, T. Eitinger, C. Ewering, M. Pötter, E. Schwartz, A. Strittmatter, I. Voß, G. Gottschalk, A. Steinbüchel, B. Friedrich and B. Bowien, *Nature Biotechnology*, 2006, **24**, 1257-1262.

58. E. Schwartz, A. Henne, R. Cramm, T. Eitinger, B. Friedrich and G. Gottschalk, *Journal of Molecular Biology*, 2003, **332**, 369-383.

59. M. Jahn, N. Crang, M. Janasch, A. Hober, B. Forsström, K. Kimler, A. Mattausch, Q. Chen, J. Asplund-Samuelsson and E. P. Hudson, *eLife*, 2021, **10**, e69019.

60. N. Pearcy, M. Garavaglia, T. Millat, J. P. Gilbert, Y. Song, H. Hartman, C. Woods, C. Tomi-Andrino, R. Reddy Bommareddy, B.-K. Cho, D. A. Fell, M. Poolman, J. R. King, K. Winzer, J. Twycross and N. P. Minton, *PLOS Computational Biology*, 2022, **18**, e1010106.

61. G. T. Little, M. Ehsaan, C. Arenas-López, K. Jawed, K. Winzer, K. Kovacs and N. P. Minton, *Microbiology Resource Announcements*, 2019, **8**, 10.1128/mra.00814-00819.

62. A. Goelzer, V. Fromion and G. Scorletti, *Automatica*, 2011, **47**, 1210-1218.

63. A. Goelzer, J. Muntel, V. Chubukov, M. Jules, E. Prestel, R. Nölker, M. Mariadassou, S. Aymerich, M. Hecker, P. Noirot, D. Becher and V. Fromion, *Metabolic Engineering*, 2015, **32**, 232-243.

64. M. Zinn, R. Durner, H. Zinn, Q. Ren, T. Egli and B. Witholt, *Biotechnology Journal*, 2011, **6**, 1240-1252.

65. E. Grousseau, E. Blanchet, S. Déléris, M. G. E. Albuquerque, E. Paul and J.-L. Uribelarrea, *Bioresource Technology*, 2013, **148**, 30-38.

66. E. Grousseau, E. Blanchet, S. Déléris, M. G. E. Albuquerque, E. Paul and J.-L. Uribelarrea, *Bioresource Technology*, 2014, **153**, 206-215.

67. H. Roh, J. S. Lee, H. I. Choi, Y. J. Sung, S. Y. Choi, H. M. Woo and S. J. Sim, *Bioresource Technology*, 2021, **327**, 124789.

68. S. Cestellos-Blanco, S. Friedline, K. B. Sander, A. J. Abel, J. M. Kim, D. S. Clark, A. P. Arkin and P. Yang, *Frontiers in Microbiology*, 2021, **12**.

69. N. Taga, K. Tanaka and A. Ishizaki, *Biotechnology and Bioengineering*, 1997, **53**, 529-533.

70. M. Zanatta, M. Lopes, E. J. Cabrita, C. E. S. Bernardes and M. C. Corvo, *Journal of CO2 Utilization*, 2020, **41**, 101225-101225.

71. M. Zanatta, N. M. Simon, F. P. dos Santos, M. C. Corvo, E. J. Cabrita and J. Dupont, *Angewandte Chemie International Edition*, 2019, **58**, 382-385.

72. P. A. Anderson, G. B. Deacon, K. H. Haarmann, F. R. Keene, T. J. Meyer, D. A. Reitsma, B. W. Skelton, G. F. Strouse and N. C. Thomas, *Inorganic Chemistry*, 1995, **34**, 6145-6157.

73. H. Li, P. H. Opgenorth, D. G. Wernick, S. Rogers, T.-Y. Wu, W. Higashide, P. Malati, Y.-X. Huo, K. M. Cho and J. C. Liao, *Science*, 2012, **335**, 1596-1596.